

# Channel water storage anomalies: A new remotely sensed measurement for global river analysis

Stephen Paul Coss<sup>1</sup>, Michael Durand<sup>1</sup>, C. K. Shum<sup>1</sup>, Yuchan Yi<sup>1</sup>, Xiao Yang<sup>2</sup>, Tamlin M Pavelsky<sup>2</sup>, Augusto Getirana<sup>3</sup>, and Dai Yamazaki<sup>4</sup>

<sup>1</sup>Ohio State University

<sup>2</sup>University of North Carolina at Chapel Hill

<sup>3</sup>NASA GSFC

<sup>4</sup>University of Tokyo

November 26, 2022

## Abstract

River channels store large volumes of water globally, critically impacting ecological and biogeochemical processes. Despite the importance of river channel storage, there is not yet an observational constraint on this quantity. We introduce a 26-year record of entirely remotely sensed volumetric channel water storage anomaly (VCWS) on 26 major world rivers. We find mainstem VCWS climatology amplitude (VCWSCA) represents an appreciable amount of basin-wide terrestrial water storage variability (median 2.2%, range 0.05-13.8% across world rivers), despite the fact that mainstem rivers themselves represent an average of just 0.2% of basin area. We find that two global river routing schemes coupled with land surface models reasonably approximate VCWSCA (within {plus minus}50%) in only 19.2 % and 23.1 % of rivers considered (by model). These findings demonstrate VCWS is a useful measurement for assessing global hydrological model performance, and for advancing understanding of spatial patterns in global hydrology.

## Hosted file

coss-gr1-2020\_supplement.docx available at <https://authorea.com/users/538734/articles/605500-channel-water-storage-anomalies-a-new-remotely-sensed-measurement-for-global-river-analysis>

1  
2  
3  
4  
5  
6  
7  
8  
9  
10  
11  
12  
13  
14  
15  
16  
17  
18  
19  
20  
21  
22

**Channel water storage anomalies: A new remotely sensed measurement for global river analysis**

**Stephen Coss<sup>1,2\*</sup>, Michael T Durand<sup>1,2</sup>, C.K. Shum<sup>1,2</sup>, Yuchan Yi<sup>1</sup>, Xiao Yang<sup>3</sup>, Tamlin Pavelsky<sup>3</sup>, Augusto Getirana<sup>4,5</sup>, Dai Yamazaki<sup>6</sup>**

<sup>1</sup>Ohio State University, Columbus, OH  
<sup>2</sup>Byrd Polar and Climate Research Center, Columbus, OH  
<sup>3</sup>University of North Carolina at Chapel Hill, Chapel Hill, NC  
<sup>4</sup>Hydrological Sciences Laboratory, NASA Goddard Space Flight Center, Greenbelt, MD  
<sup>5</sup>Science Applications International Corporation, Greenbelt, MD, United States  
<sup>6</sup>Institute of Industrial Science, The University of Tokyo, Meguro-ku, Tokyo, Japan

Corresponding author: Stephen Coss ([coss.31@osu.edu](mailto:coss.31@osu.edu))

**Key Points:**

- We introduce a 26-year record of entirely remotely sensed volumetric channel water storage anomaly.
- Storage climatology amplitude represents (0.05-13.8%) terrestrial water storage variability but just 0.2% of basin area.
- This new measurement can be used to analyze river spatial storage patterns in a way that was previously unprecedented.

23

24 **Abstract**

25 River channels store large volumes of water globally, critically impacting ecological and  
26 biogeochemical processes. Despite the importance of river channel storage, there is not yet an  
27 observational constraint on this quantity. We introduce a 26-year record of entirely remotely  
28 sensed volumetric channel water storage anomaly (VCWS) on 26 major world rivers. We find  
29 mainstem VCWS climatology amplitude (VCWSCA) represents an appreciable amount of basin-  
30 wide terrestrial water storage variability (median 2.2%, range 0.05-13.8% across world rivers),  
31 despite the fact that mainstem rivers themselves represent an average of just 0.2% of basin  
32 area. We find that two global river routing schemes coupled with land surface models  
33 reasonably approximate VCWSCA (within  $\pm 50\%$ ) in only 19.2 % and 23.1 % of rivers considered  
34 (by model). These findings demonstrate VCWS is a useful measurement for assessing global  
35 hydrological model performance, and for advancing understanding of spatial patterns in global  
36 hydrology.

37 **Plain Language Summary**

38 Rivers are a critical part of global hydrology, but until now the variation in how much water  
39 rivers store has not been observed directly on the global scale. We created a 25 year record of  
40 this measurement across 26 of the world's largest rivers. We found that the storage variation in  
41 river main channels can represent up to 13% of the total water variation in a river basin despite  
42 only representing 0.2% of the total surface area. We also find that current methods to estimate  
43 this quantity through modeling (global river routing schemes coupled with land surface models)  
44 are only representing this quantity within 50% of the measured value on between 19.2% to  
45 23.1% of the rivers we studied. This demonstrates that this new measurement has value in  
46 assessing model performance and advancing the way we think about how rivers function as  
47 water storage vessels.

## 48 **1 Introduction**

49 While spaceborne sensors have revolutionized our understanding of global hydrology, some  
50 terms in the global water cycle remain poorly observed (Lettenmaier et al., 2015). For example,  
51 while the Gravity Recovery And Climate Experiment (GRACE; Tapley et al., 2004, 2019) and  
52 GRACE Follow-On satellite missions have provided invaluable measurements of global water  
53 storage variability (Rodell et al., 2018), they measure the total terrestrial water storage (TWS)  
54 anomaly, but do not provide information on the dynamics of individual TWS components such  
55 as soil moisture, snow, ground and surface water.

56 Surface water storage (SWS) in natural and artificial reservoirs, floodplains, wetlands and river  
57 channels is critical to human society and ecosystems, but a complete picture of surface water  
58 storage dynamics from remote sensing measurements has remained elusive (Döll et al., 2012;  
59 Oki & Kanae, 2006). Getirana et al. (2017) modeled SWS globally (neglecting anthropogenic  
60 impacts ) and estimated that on average, SWS contributes just 8% of overall TWS variability; it is  
61 thus difficult to estimate SWS by difference, i.e. by subtracting estimates of other storage terms  
62 from GRACE TWS measurements (e.g., Llovel et al., 2010; Swenson et al., 2008; Syed et al.,  
63 2008). Remote sensing measurements have shed light on storage change in major world  
64 floodplains (Papa et al., 2013; 2015), and on storage in global lakes and reservoirs (Gao et al.,  
65 2012; Tortini et al., 2020). However, an observation-based quantification of storage change in  
66 rivers has been lacking.

67 A comprehensive dataset of observations of volumetric changes of water in rivers has not been  
68 previously presented, despite the potential value of such observations and the relative  
69 simplicity with which such variations can be measured. Time-varying river storage changes

70 would have value in understanding global water balance and within-watershed variations in  
71 TWS. Kim et al. (2009) demonstrated that rivers are major contributors (between 0 and 70%) to  
72 TWS variation by modeling river (channel and sub-surface), snow and soil moisture  
73 contributions to TWS; however, their work did not separate surface water from underground  
74 flow. As noted above, Getirana et al. (2017) found that in most basins the SWS:TWS variability  
75 ratio was low, but its maximum value (27%) for the Amazon basin indicated that, for some  
76 regions, surface water can play a major role in storage dynamics. We hypothesize that rivers  
77 are frequently hotspots of water storage variability, a part of watersheds where much greater  
78 water storage change tends to occur than elsewhere. E.g., major rivers typically exhibit  
79 seasonal water level measuring several meters, while GRACE TWS seasonal changes are usually  
80 < 100 mm across the entire basin. The global measurements of river storage presented in this  
81 paper let us quantify these dynamics and help validate model estimates of rivers, which  
82 increasingly simulate global river processes (Emery et al., 2018; Getirana, Kumar, et al., 2017;  
83 Yamazaki et al., 2011). Finally, storage variations of water in rivers is crucial for ecological and  
84 biogeochemical processes. Indeed, storage variations are driven by the same basic hydrologic  
85 quantities that drive hyporheic exchange: variations in river depth and surface area. Because  
86 water surface elevations (Calmant et al., 2008; Coss et al., 2020; Tourian et al., 2016) and river  
87 surface water extent (Allen & Pavelsky, 2018; Huang et al., 2012; Yamazaki et al., 2015) datasets  
88 exist, long-term storage variations in rivers can be measured directly, by simply combining  
89 water surface elevation (WSE) and width observations, both of which are measured entirely  
90 from satellite platforms.

91 Here, we present the first published data product of volumetric river channel water storage  
92 anomaly (VCWS) over 26 of the world’s largest rivers using remotely sensed river WSEs and  
93 widths in the Global River Radar Altimetry Time Series 1 Kilometer Daily (GRRATS1kd, Coss et  
94 al., 2019a). In the context of VCWS we define “anomaly” as the difference between a value at a  
95 particular time, and some reference time,  $t$  (e.g. the first date in our dataset). Storage change  
96 is the time derivative of storage, and can be calculated from the time derivative of the storage  
97 anomaly. GRACE TWS is also either a storage anomaly or storage change measurement; in this  
98 paper we use “TWS” to refer to storage anomaly. We use the new GRRATS1kd dataset to  
99 address three questions: How large are storage variations within river mainstems compared to  
100 basin storage variations measured by GRACE? What controls spatial patterns of storage  
101 variations in rivers? How do measured river storage variations compare to modeled values?

## 102 **2 Methods and Datasets**

103  
104 GRRATS1kd is a one kilometer-one day resolution interpolated dataset spanning 26 of the  
105 world’s largest rivers (Coss et al., 2019a); a list of the rivers is given in Table 1. GRRATS1kd  
106 comprises satellite altimetry measurements of river WSE interpolated to 1 km daily resolution,  
107 and VCWS estimates computed from interpolated WSE and width. The virtual station data  
108 GRRATS (Coss et al., 2019b), is further described in (Coss et al., 2020). In this section, we briefly  
109 describe the datasets and major steps used to compute VCWS.

110 The primary input datasets used to create GRRATS1kd are measurements of river WSE at the  
111 intersection of radar altimeter ground tracks and rivers, known as virtual stations (VS)  
112 (GRRATS, described by (Coss et al., 2020)), and river width measurements obtained using

113 RivWidthCloud, a Landsat processing algorithm for measuring river width based on Google  
 114 Earth Engine (Yang et al., 2019). We use a total of 914 GRRATS VSs spanning 1992-2018  
 115 leveraging seven altimeters (ERS-1, TOPEX/Poseidon, ERS-2, JASON-1, Envisat, OSTM/Jason-2,  
 116 Jason-3). (<https://doi.org/10.5067/PSGRA-SA2V1>). Note that Coss et al. (2020) describes  
 117 version 1 of GRRATS, which included only 2 altimeters. The VSs processed by Coss et al. (2020)  
 118 included all locations on ocean-draining main-stem rivers with a mean width of 900m or  
 119 greater. The 26 rivers used for this study are those with enough data density to interpolate a  
 120 daily 1km resolution WSE (26 of 39). RivWidthCloud was used to process a total of 53,924  
 121 Landsat images in order to generate a total of 115.2 million (2.2 million after 1km averaging and  
 122 quality filtering) channel width measurements.

123 In GRRATS1kd, VCWS is computed as follows. First, we statistically reprocess the GRRATS VS  
 124 data to remove outliers using a moving window  $t$ -test (Coss et al., 2020). Second, we  
 125 interpolate VS WSEs to 1 km daily resolution, by grouping VS data by altimeter constellation,  
 126 bilinear interpolation of anomaly on a flow distance-time grid, smoothing, adding back a digital  
 127 elevation model (DEM) value to convert back to absolute WSE (DEM selection is identical to the  
 128 description in Coss et al., (2020)), and finally forcing WSEs to decrease downriver at each time  
 129 step. Third, for each 1 km location downstream, we create a piecewise-linear relationship  
 130 between WSE and width ( $W$ ) as described in the supplemental material (S1). These piecewise  
 131 linear relationships between  $W$  and WSE can be represented as:  $= f_x(WSE)$  .

132 VCWS in units of  $\text{km}^3$  can be calculated by integrating the  $W$ -WSE relationships at location  $x$ :

$$133 \quad VCWS_{x,t} = \Delta_x \int_{WSE_{x,t1}}^{WSE_{x,t}} f_x(WSE) dWSE, \quad (1)$$

134 where the  $x$  subscript indicates that these values (as well as the piecewise linear relationships  
135 between WSE and  $W$ ) are specific to one 1 km segment, and  $\Delta_x$  is the segment resolution, and  
136  $t_1$  is the initial time in the series (typically a date in April 1992). Thus, VCWS has dimensions of  
137 cubic volume, and can be thought of as the product of river cross-sectional area anomaly (the  
138 integral term in Eq. 1, units of  $m^2$ ) and  $\Delta_x$ . When we present timeseries of river total VCWS  
139 values, we simply sum  $VCWS_{x,t}$  over all spatial locations  $x$  (Figure 1A). Note that reservoirs are  
140 flagged and removed.

141 For model comparisons (described below)), we analyzed data from two global SWS datasets.  
142 Both the Hydrological Modeling and Analysis Platform (Getirana et al., 2012; Getirana, Peters-  
143 Lidard, et al., 2017) and the Catchment-based Macro-scale Floodplain model (Yamazaki et al.,  
144 2011; 2014) are river routing schemes capable of simulating river and floodplain dynamics.  
145 They are forced with surface runoff and baseflow simulated by land surface models. For the  
146 data we analyzed, temporal resolution is daily, spatial resolution is  $1^\circ$  ( $\sim 100$  km) for HyMAP and  
147  $0.1^\circ$  ( $\sim 10$  km) for CaMa-Flood, and the temporal domain is 2002-2017 for HyMAP and 2000-  
148 2011 for CaMa-Flood.

149

150 Below, we present three separate analyses of climatologies constructed from our data. First we  
151 compare with GRACE long-term average TWS climatology. The GRACE data presented is from  
152 the Center for Space Research at the University of Texas at Austin (  
153 <http://www2.csr.utexas.edu/grace>). The Data are monthly Mascon solutions spanning 2002-  
154 2018, with a 0.25 degree resolution, with an 11 month gap from July of 2017- May of 2018  
155 between GRACE missions (Hosseini-Moghari et al., 2020; Save et al., 2016). For each basin, we

156 create a 26 year VCWS climatology (VCWSC) summed over the length of the river (Figure 2B).  
157 We then measure the amplitude of VCWSC (VCWSCA). Some analyses below present VCWSCA  
158 normalized by basin drainage area (i.e. we divide the VCWSC amplitude value by the basin  
159 drainage area); we refer to this quantity as channel water storage (CWS) following the  
160 definition for GRACE TWS, CWS is presented with units of mm, and is comparable to GRACE.  
161 Figure 1 for example, shows the Mississippi VCWSCA is  $7.12 \text{ km}^3$  while the drainage area is  
162  $3,244,506 \text{ km}^2$ . Dividing VCWSCA by drainage area results in a CWS of  $\sim 2.2 \text{ mm}$ . Basin areas are  
163 from the United Nations Chief Executive Officer Water Mandate (2016) and World Bank Major  
164 River Basins (2017) datasets.

165 In our discussion of the relationship of CWS to GRACE we reference mean slope data from  
166 (Coss et al., 2019b, 2020) and calculate an aridity index from net radiation from Clouds and the  
167 Earth's Radiant Energy System (CERES; Loeb et al., 2018; Wielicki et al., 1996) and Global  
168 Precipitation Climatology Project (GPCP; Adler et al., 2003).

169 Second, we relate VCWSCA, mean river width, and basin area at 1km resolution and test if  
170 different basin area groups have different CWSA/width relationships. To compare VCWSCA  
171 regimes, we relate our VCWSCA data to basin drainage area from Frasson et al., (2019). We first  
172 distinguished groups by large increases in flow accumulation to avoid comparison across large  
173 tributaries. We then re-assimilate any divisions that did not achieve a change in basin drainage  
174 area  $> 10\%$ . Finally, we plot VCWSCA and mean width by 1 km section and perform a simple least  
175 squares linear regression on each group. To verify that their slopes are appreciably different, we  
176 use the Z test outlined in Paternoster et al., (1998), with a threshold of 2 for failing the null  
177 hypotheses (slopes are the same). Third, we compare with global models by scaling the

178 GRRATS1kd data up to the model grid resolution (1 or 0.1 degrees), by summing all of our 1 km  
179 VCWS data points that fall within each model grid cell. We then examine two criteria: 1) The  
180 VCWSCA for all cells overlapping measured channel; 2) Correlation coefficient of each model  
181 cell, with the average measured VCWSCA from those measured sections that fell within the cell.

### 182 **3 Results and Discussion**

183       3.1 The magnitude of main stem CWS as it relates to GRACE TWS  
184 CWS ranges from 0.02 mm to 21.9 mm (on the Zambezi and Ayeyarwada rivers, respectively),  
185 with a mean value of 5.36 mm (Figure 2). As expected, the largest values are primarily from  
186 tropical basins. Table 1 shows the ratio of CWS compared with GRACE TWS (CWS:TWS ratio  
187 hereafter) climatology data constructed from Save et al. (2016) for each of the study river  
188 basins Note that for GRACE comparison the Ganges and Brahmaputra basins have been  
189 combined. CWS:TWS ratio ranges from 0.05% to 13.8% (on the Zambezi and Uruguay Rivers  
190 respectively), with an average of 3.5 % of GRACE TWS being measured in river main stems. That  
191 the main stem river contribute an average of several percent of all basin storage variability is  
192 perhaps surprising when considering that mainstem rivers constitute on average just 0.2% of  
193 total basin area (Table 1). This analysis highlights rivers as storage hotspots, parts of major  
194 drainage basins where an oversized fraction of storage variation takes place.  
195 CWS:TWS varies over two orders of magnitude on study rivers, evincing tremendous diversity  
196 across global basins in rivers' role in overall basin storage. As the mainstem combines both  
197 upstream hydrologic processes and river hydraulics, we explored the role of basin aridity index  
198 (AI, defined as the ratio of long-term average potential evaporation to precipitation; see  
199 (McMahon et al., 2013) and mainstem slope in the CWS:TWS. We hypothesized that basins with

200 high AI would have a lower total runoff, and thus a lower CWS:TWS ratio, and that basins with  
201 low slope would likely have slower flow velocities, longer channel residence times, and thus  
202 larger CWS:TWS ratios. Note AI is presented for only 18 of the 25 basins due to data availability.  
203 Overall, we found that these hypotheses bear out in generally, but a predictive relationship was  
204 not identified. Specifically, we found that all three rivers with a CWS:TWS ratio above 5.5%  
205 were both low slope (<2727 cm/km) and low AI (<0.88). Similarly, 6 of the 8 rivers with a  
206 CWS:TWS ratio below 2% had a relatively high AI (>1). Neither slope nor AI correlated linearly  
207 with the CWS :TWS ratio, however. For example, the Tocantins and St Lawrence rivers have low  
208 AI (< 1), but still have a but still have a low CWS:TWS ratio (approximately 1%). We speculate  
209 that other factors such as spatiotemporal variability of precipitation patterns and snow storage  
210 also play a role; the Congo, for instance has a two peak hydrograph due to its position under  
211 the inter-tropical convergence zone (e.g., Alsdorf et al., 2016)), limiting the predictive power of  
212 the AI on basin hydrology (e.g. McMahon et al., 2013).). The human influence due to dams, and  
213 storage of water in large floodplains likely also play a role. As a final effort to understand  
214 CWS:TWS ratio, we hypothesized simply that basins with larger proportion of their surface area  
215 represented by the mainstem would similarly also have a larger CWS:TWS ratio. A linear  
216 relationship was identified between these quantities (see Table 1), with  $R^2 = 0.54$  and  $p = 0$ , but  
217 this is in part due to the Uruguay river, which can be considered an outlier, with CWS :TWS of  
218 nearly 14%. Excluding the Uruguay,  $R^2 = 0.1717$  and  $p = 0.042$ . This result means that the  
219 correlation between measured area and CWS:TWS ratio is only significant, when the Uruguay is  
220 included. In summary, rivers are storage hotspots within major drainage basins, manifesting  
221 orders of magnitude larger storage variability than on average. There is significant variability

222 among river basins in how large a role the mainstem plays in basinwide storage dynamics,  
223 however, it is unclear what factors drive this variability.

### 224 3.2 VCWSCA Regimes

225 While we might expect VCWSCA to increase monotonically with distance downstream, this is  
226 frequently not the case. As we can see from the Congo (Figure 2) we sometimes see the  
227 opposite, and most frequently find that VCWSCA hotspots occur in a variety of locations on the  
228 mainstem of a river (Amazon, Mississippi). Controls on spatial patterns of VCWSCA in rivers are  
229 diverse and complex. The Amazon, for example, has large flood plain lakes that suppress  
230 surface elevation variation (Bonnet et al., 2008). In an effort to quantify this phenomenon, we  
231 compare the relationship between VCWSCA and mean channel width, and basin drainage area  
232 at 1 km resolution for 19 of the rivers for which drainage area data are available from Frasson  
233 et al. (2019). Generally, as width increases, the VCWSCA increases as well (Figure 4). This is not  
234 a uniformly applicable principle, however. Relative Amplitude (e.g. Figure 1a) does not increase  
235 uniformly in all rivers as they widen downstream. This means consideration of variation in  
236 space is critical for understanding individual rivers' VCWS signature. However, some rivers  
237 further show distinct relationships that can be explained by drainage area. Because of the river  
238 sections being analyzed, only 15 of the 19 rivers can be subdivided into 2 or more  
239 distinguishable (drainage area difference > 10%) groups. For these 15 rivers, we are able to  
240 isolate two distinct patterns in the relationship between VCWSCA, mean width, and drainage  
241 area. For the first pattern (exemplified by Figure 4a), the slope of the VCWSCA: width  
242 relationship does not change with drainage area; for the second pattern (e.g. Figure 4b), the  
243 slope changes significantly. We find that 9 rivers show significant changes their VCWSCA: width

244 relationship with variation in drainage area (Table 1). While the basins with changing slope are  
245 broadly geographically distributed, all but one of the non-changing slope basins (Columbia) are  
246 near-equatorial (within 30°N of the equator). One possible explanation for this result is that as  
247 noted above, large floodplain lakes and floodplain-mainstem interaction in many equatorial  
248 basins control water level variation so dramatically, that changes in drainage area downstream  
249 produce no distinct change in the spatial patterns of storage variations.

### 250 3.3 Model Comparisons

251 While comparison of GRRATS1kd with HyMAP and CaMa-flood reveals promising similarity  
252 between model and measured data on some rivers (Figure 3), HyMAP and CaMa-flood  
253 reasonably approximate VCWSCA in 23.1% and 19.2% of the rivers respectively. We define  
254 “reasonable” as having a climatology amplitude within  $\pm 50\%$  (Wrzesien et al., 2017). We show  
255 the cumulative distribution function of these amplitude comparisons for all rivers in Figure 3D  
256 (amplitude ratios  $< 4$ ) to provide a more comprehensive view of these data. With few  
257 exceptions, the model and measurements are generally in phase; Figure 3c is an exception. To  
258 assess the capabilities of the models to represent spatial patterns in VCWSCA, we also  
259 compared the Spatial Normalized VCWSCA, that is the spatial series of measured and modeled  
260 VCWSCA, after gridding GRRATS1kd onto the model grid. In general, we found that the models  
261 represent the seasonal amplitude better than spatial patterns. At the grid cell level, we  
262 compared seasonal amplitude from the models and our measurements. For CaMa-flood we find  
263 that 50% of rivers (26.9% that were statistically significant) have an average cell correlation  $> 0$   
264 (12%  $> 0.5$ ), with a maximum value of 0.8. HyMAP results show 62% of rivers (12.5% that were  
265 statistically significant) with an average cell correlation  $> 0$  (15%  $> 0.5$ ), with a maximum value of

266 0.9. Overall these results demonstrate that while models often represent the magnitude of this  
267 signal well, they tend to misrepresent the location of the water. Variation in scaling and model  
268 precipitation inputs could be responsible for many of the differences we see between the  
269 models and measured values. In some extreme cases, we looked at the VCWS components  
270 (width and height variation) from the model in greater depth and found that the standard  
271 deviation of height is often much higher than measured. It is possible that overestimation of  
272 height variation and simplified width variation heavily impact where this variation happens in  
273 the models.

## 274 **5 Conclusions**

275 Here we use a new remote sensing dataset (VCWS) to explore the role of major world rivers in  
276 the global water cycle. We find that rivers are storage hotspots, parts of major drainage basins  
277 where an exceptionally large fraction of total storage variation takes place. Specifically, by  
278 comparing our dataset with GRACE, we showed that the mainstem river accounted for a highly  
279 variable percentage (0.05%-13.8%) of all water storage changes within the basin, among the  
280 drainage basins analyzed. We hypothesize that a complex array of factors, including basin  
281 hydrology and river hydraulics, govern the ratio of river to total water storage change among  
282 basins; our preliminary results show that basic factors such as basin-averaged aridity index and  
283 river slope do not explain these variations.

284 We find that within-river spatial patterns in channel water storage climatology anomaly are  
285 highly complex, and do not simply increase monotonically with distance downstream as we  
286 hypothesized they would. Frequently the opposite pattern emerges, though highly variable  
287 hotspot patterns are most common. We find that while the width and channel water storage

288 climatology relationship generally changes with flow accumulation (expected behavior), this is  
289 not always the case (40% do not). The expected behavior generally occurs in near equatorial  
290 basins, highlighting that complex hydraulics (tributary backwater, ice jams etc.) might be a  
291 much more significant cause of storage variation in rivers at higher latitudes. Third, we find  
292 global river routing schemes tend to capture the amplitude of river storage variations more  
293 successfully than they represent the spatial nature of how rivers store their water. We find that  
294 models represent channel water storage climatology anomaly reasonably ( $\pm 50\%$ ) in only 19.2%  
295 and 23.1% of rivers considered (by model). We also find that model cells significantly correlate  
296 spatially with measured data on just 26% and 12.5% of rivers (by model). We did not diagnose  
297 the cause of these discrepancies, but hypothesize that effects of anthropogenic management  
298 (not simulated by the models) play an important role. Future work should explore assimilation  
299 of channel water storage into such models, as well as integration with existing datasets  
300 measuring floodplains and reservoirs. Such work is even more important, given recent and  
301 future datasets that represent improved height and inundated area measurements from  
302 sensors such as Planet, Sentinel -2, Landsat 8+9 and the upcoming SWOT mission (Boshuizen et  
303 al., 2014; Drusch et al., 2012; Fu et al., 2009; MarkhamM et al., 2019; Roy et al., 2014).

#### 304 Acknowledgments and Data

305 The authors report no conflicts of interest.

306 The data used in this study (DOI: 10.5067/PSGRA-DA2V2) is available on the NASA  
307 PO.DAAC

308 ([https://podaac.jpl.nasa.gov/dataset/PRESWOT\\_HYDRO\\_GRRATS\\_L2\\_DAILY\\_VIRTUAL\\_S  
309 TATION\\_HEIGHTS\\_V2?ids=&values=](https://podaac.jpl.nasa.gov/dataset/PRESWOT_HYDRO_GRRATS_L2_DAILY_VIRTUAL_S<br/>309 TATION_HEIGHTS_V2?ids=&values=)).

310

311 This work was supported by a NASA FINESST award (GRT00054946).

312

313 **References**

- 314 Allen, G. H., & Pavelsky, T. M. (2018). Global extent of rivers and streams. *Science*, *361*(6402),  
315 585. <https://doi.org/10.1126/science.aat0636>
- 316 Alsdorf, D., Beighley, E., Laraque, A., Lee, H., Tshimanga, R., O'Loughlin, F., et al. (2016).  
317 Opportunities for hydrologic research in the Congo Basin. *Reviews of Geophysics*, *54*(2),  
318 378–409. <https://doi.org/10.1002/2016RG000517>
- 319 Bonnet, M. P., Barroux, G., Martinez, J. M., Seyler, F., Moreira-Turcq, P., Cochonneau, G., et al.  
320 (2008). Floodplain hydrology in an Amazon floodplain lake (Lago Grande de Curuaí).  
321 *Journal of Hydrology*, *349*(1), 18–30. <https://doi.org/10.1016/j.jhydrol.2007.10.055>
- 322 Boshuizen, C., Mason, J., Klupar, P., & Spanhake, S. (2014). Results from the planet labs flock  
323 constellation.
- 324 Calmant, S., Seyler, F., & Cretaux, J. F. (2008). Monitoring continental surface waters by  
325 satellite altimetry. *Surveys in Geophysics*, *29*(4–5), 247–269.
- 326 CEO Water Mandate. (2016). Retrieved April 22, 2020, from  
327 <http://ceowatermandate.org/riverbasins>.
- 328 Coss, S., Durand, M., Lettenmaier, D., Yi, Y., Jia, Y., Guo, Q., et al. (2019a). Pre SWOT  
329 Hydrology GRRATS Daily River Heights and Storage Version 2. *PO.DAAC*.  
330 <https://doi.org/10.5067/PSGRA-DA2V2>
- 331 Coss, S., Durand, M., Lettenmaier, D., Yi, Y., Jia, Y., Guo, Q., et al. (2019b). Pre SWOT  
332 Hydrology GRRATS Virtual Station River Heights Version 2. NASA Physical  
333 Oceanography DAAC. <https://doi.org/10.5067/PSGRA-SA2V2>
- 334 Coss, S., Durand, M., Yi, Y., Jia, Y., Guo, Q., Tuozzolo, S., et al. (2020). Global River Radar  
335 Altimetry Time Series (GRRATS): new river elevation earth science data records for the

- 336 hydrologic community. *Earth Syst. Sci. Data*, 12(1), 137–150.  
337 <https://doi.org/10.5194/essd-12-137-2020>
- 338 Döll, P., Hoffmann-Dobrev, H., Portmann, F. T., Siebert, S., Eicker, A., Rodell, M., et al. (2012).  
339 Impact of water withdrawals from groundwater and surface water on continental water  
340 storage variations. *Journal of Geodynamics*, 59–60, 143–156.  
341 <https://doi.org/10.1016/j.jog.2011.05.001>
- 342 Drusch, M., Del Bello, U., Carlier, S., Colin, O., Fernandez, V., Gascon, F., et al. (2012).  
343 Sentinel-2: ESA’s optical high-resolution mission for GMES operational services.  
344 *Remote Sensing of Environment*, 120, 25–36.
- 345 Emery, C. M., Paris, A., Biancamaria, S., Boone, A., Calmant, S., Garambois, P.-A., & da Silva,  
346 J. S. (2018). Large-scale hydrological model river storage and discharge correction using  
347 a satellite altimetry-based discharge product. *Hydrology and Earth System Sciences*,  
348 22(4), 2135.
- 349 Frasson, R. P. de M., Pavelsky, T. M., Fonstad, M. A., Durand, M. T., Allen, G. H., Schumann,  
350 G., et al. (2019). Global relationships between river width, slope, catchment area,  
351 meander wavelength, sinuosity, and discharge. *Geophysical Research Letters*, 46(6),  
352 3252–3262.
- 353 Fu, L.-L., Alsdorf, D., Rodriguez, E., Morrow, R., Mognard, N., Lambin, J., et al. (2009). The  
354 SWOT (Surface Water and Ocean Topography) mission: spaceborne radar interferometry  
355 for oceanographic and hydrological applications. Presented at the OCEANOBS’09  
356 Conference, Citeseer.

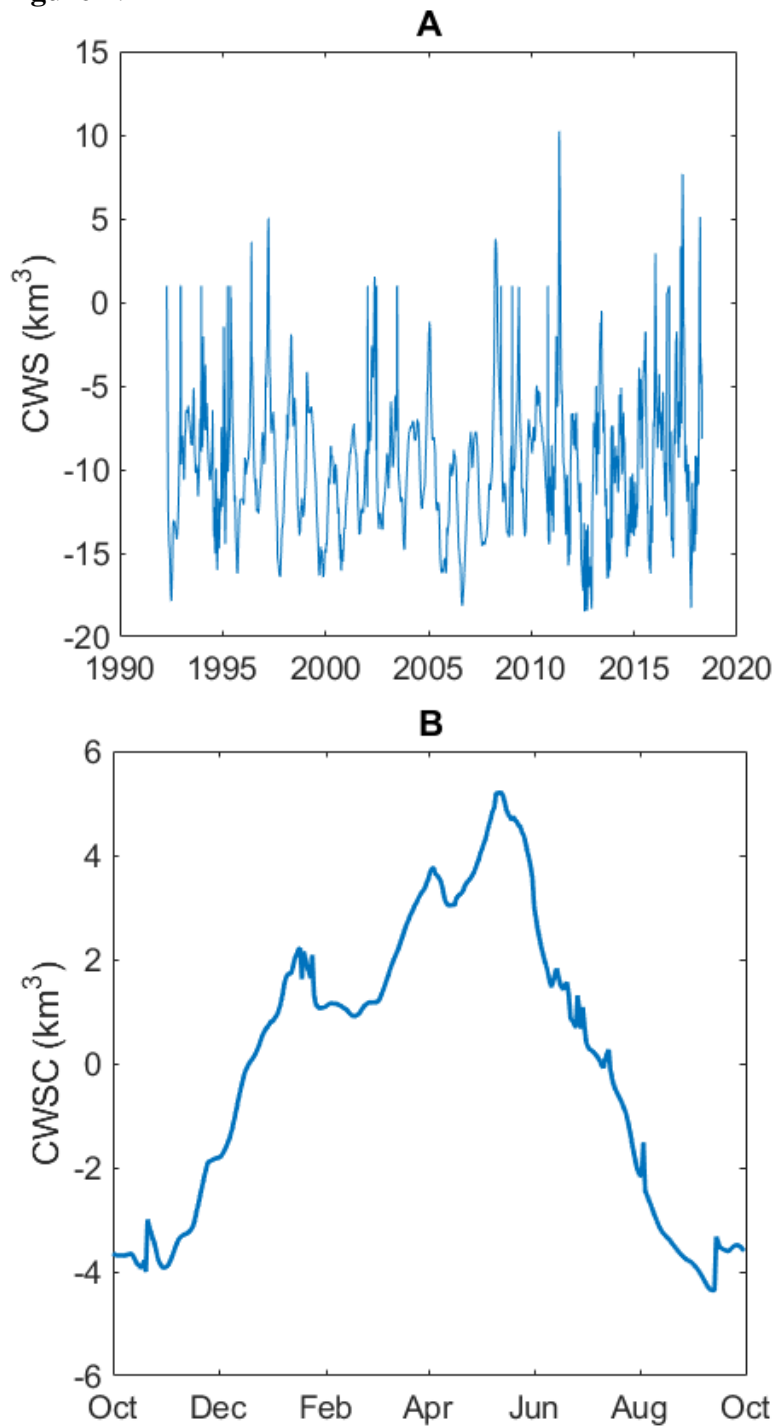
- 357 Gao, H., Birkett, C., & Lettenmaier, D. P. (2012). Global monitoring of large reservoir storage  
358 from satellite remote sensing. *Water Resources Research*, 48(9).  
359 <https://doi.org/10.1029/2012WR012063>
- 360 Getirana, A., Boone, A., Yamazaki, D., Decharme, B., Papa, F., & Mognard, N. (2012). The  
361 hydrological modeling and analysis platform (HyMAP): Evaluation in the Amazon basin.  
362 *Journal of Hydrometeorology*, 13(6), 1641–1665.
- 363 Getirana, A., Kumar, S., Girotto, M., & Rodell, M. (2017). Rivers and Floodplains as Key  
364 Components of Global Terrestrial Water Storage Variability. *Geophysical Research*  
365 *Letters*, 44(20), 10,359–10,368. <https://doi.org/10.1002/2017GL074684>
- 366 Getirana, A., Peters-Lidard, C., Rodell, M., & Bates, P. D. (2017). Trade-off between cost and  
367 accuracy in large-scale surface water dynamic modeling. *Water Resources Research*,  
368 53(6), 4942–4955. <https://doi.org/10.1002/2017WR020519>
- 369 Hosseini-Moghari, S.-M., Araghinejad, S., Ebrahimi, K., Tang, Q., & AghaKouchak, A. (2020).  
370 Using GRACE satellite observations for separating meteorological variability from  
371 anthropogenic impacts on water availability. *Scientific Reports*, 10(1), 15098.  
372 <https://doi.org/10.1038/s41598-020-71837-7>
- 373 Huang, S., Li, J., & Xu, M. (2012). Water surface variations monitoring and flood hazard  
374 analysis in Dongting Lake area using long-term Terra/MODIS data time series. *Natural*  
375 *Hazards*, 62(1), 93–100. <https://doi.org/10.1007/s11069-011-9921-6>
- 376 Kim, H., Yeh, P. J., Oki, T., & Kanae, S. (2009). Role of rivers in the seasonal variations of  
377 terrestrial water storage over global basins. *Geophysical Research Letters*, 36(17).

- 378 Lettenmaier, D. P., Alsdorf, D., Dozier, J., Huffman, G. J., Pan, M., & Wood, E. F. (2015).  
379 Inroads of remote sensing into hydrologic science during the WRR era. *Water Resources*  
380 *Research*, 51(9), 7309–7342.
- 381 Llovel, W., Becker, M., Cazenave, A., Crétaux, J.-F., & Ramillien, G. (2010). Global land water  
382 storage change from GRACE over 2002–2009; Inference on sea level. *Comptes Rendus*  
383 *Geoscience*, 342(3), 179–188.
- 384 Loeb, N. G., Su, W., Doelling, D. R., Wong, T., Minnis, P., Thomas, S., & Miller, W. F. (2018).  
385 5.03 - Earth's Top-of-Atmosphere Radiation Budget. In S. Liang (Ed.), *Comprehensive*  
386 *Remote Sensing* (pp. 67–84). Oxford: Elsevier. [https://doi.org/10.1016/B978-0-12-](https://doi.org/10.1016/B978-0-12-409548-9.10367-7)  
387 [409548-9.10367-7](https://doi.org/10.1016/B978-0-12-409548-9.10367-7)
- 388 Major River Basins Of The World. (2017, July 24). Retrieved January 1, 2018, from  
389 <https://datacatalog.worldbank.org/dataset/major-river-basins-world>
- 390 Markham, B., Barsi, J., Donley, E., Efremova, B., Hair, J., Jenstrom, D., et al. (2019). Landsat  
391 9: Mission status and prelaunch instrument performance characterization and calibration  
392 (pp. 5788–5791). Presented at the IGARSS 2019-2019 IEEE International Geoscience  
393 and Remote Sensing Symposium, IEEE.
- 394 McMahon, T., Laaha, G., Parajka, J., Peel, M., Savenije, H., Sivapalan, M., et al. (2013).  
395 Prediction of annual runoff in ungauged basins.
- 396 Oki, T., & Kanae, S. (2006). Global hydrological cycles and world water resources. *Science*,  
397 *313*(5790), 1068–1072.
- 398 Papa, F., Frappart, F., Güntner, A., Prigent, C., Aires, F., Getirana, A. C. V., & Maurer, R.  
399 (2013). Surface freshwater storage and variability in the Amazon basin from multi-

- 400 satellite observations, 1993–2007. *Journal of Geophysical Research: Atmospheres*,  
401 118(21), 11,951–11,965. <https://doi.org/10.1002/2013JD020500>
- 402 Papa, F., Frappart, F., Malbeteau, Y., Shamsudduha, M., Vuruputur, V., Sekhar, M., et al.  
403 (2015). Satellite-derived surface and sub-surface water storage in the Ganges–  
404 Brahmaputra River Basin. *Groundwater Systems of the Indian Sub-Continent*, 4, 15–35.  
405 <https://doi.org/10.1016/j.ejrh.2015.03.004>
- 406 Paternoster, R., Brame, R., Mazerolle, P., & Piquero, A. (1998). Using the correct statistical test  
407 for the equality of regression coefficients. *Criminology*, 36(4), 859–866.
- 408 Rodell, M., Famiglietti, J. S., Wiese, D. N., Reager, J. T., Beaudoing, H. K., Landerer, F. W., &  
409 Lo, M.-H. (2018). Emerging trends in global freshwater availability. *Nature*, 557(7707),  
410 651–659. <https://doi.org/10.1038/s41586-018-0123-1>
- 411 Roy, D. P., Wulder, M. A., Loveland, T. R., Woodcock, C., Allen, R. G., Anderson, M. C., et al.  
412 (2014). Landsat-8: Science and product vision for terrestrial global change research.  
413 *Remote Sensing of Environment*, 145, 154–172.
- 414 Save, H., Bettadpur, S., & Tapley, B. D. (2016). High-resolution CSR GRACE RL05 mascons.  
415 *Journal of Geophysical Research: Solid Earth*, 121(10), 7547–7569.
- 416 Swenson, S., Famiglietti, J., Basara, J., & Wahr, J. (2008). Estimating profile soil moisture and  
417 groundwater variations using GRACE and Oklahoma Mesonet soil moisture data. *Water*  
418 *Resources Research*, 44(1).
- 419 Syed, T. H., Famiglietti, J. S., Rodell, M., Chen, J., & Wilson, C. R. (2008). Analysis of  
420 terrestrial water storage changes from GRACE and GLDAS. *Water Resources Research*,  
421 44(2).

- 422 Tapley, B. D., Bettadpur, S., Watkins, M., & Reigber, C. (2004). The gravity recovery and  
423 climate experiment: Mission overview and early results. *Geophysical Research Letters*,  
424 *31*(9).
- 425 Tapley, B. D., Watkins, M. M., Flechtner, F., Reigber, C., Bettadpur, S., Rodell, M., et al.  
426 (2019). Contributions of GRACE to understanding climate change. *Nature Climate*  
427 *Change*, *9*(5), 358–369.
- 428 Tortini, R., Noujdina, N., Yeo, S., Ricko, M., Birkett, C. M., Khandelwal, A., et al. (2020).  
429 Satellite-based remote sensing data set of global surface water storage change from 1992  
430 to 2018. *Earth System Science Data*, *12*(2), 1141–1151. [https://doi.org/10.5194/essd-12-](https://doi.org/10.5194/essd-12-1141-2020)  
431 [1141-2020](https://doi.org/10.5194/essd-12-1141-2020)
- 432 Tourian, M., Tarpanelli, A., Elmi, O., Qin, T., Brocca, L., Moramarco, T., & Sneeuw, N. (2016).  
433 Spatiotemporal densification of river water level time series by multimission satellite  
434 altimetry. *Water Resources Research*.
- 435 Wielicki, B. A., Barkstrom, B. R., Harrison, E. F., Lee, R. B., III, Smith, G. L., & Cooper, J. E.  
436 (1996). Clouds and the Earth's Radiant Energy System (CERES): An Earth Observing  
437 System Experiment. *Bulletin of the American Meteorological Society*, *77*(5), 853–868.  
438 [https://doi.org/10.1175/1520-0477\(1996\)077<0853:CATERE>2.0.CO;2](https://doi.org/10.1175/1520-0477(1996)077<0853:CATERE>2.0.CO;2)
- 439 Wrzesien, M. L., Durand, M. T., Pavelsky, T. M., Howat, I. M., Margulis, S. A., & Huning, L. S.  
440 (2017). Comparison of methods to estimate snow water equivalent at the mountain range  
441 scale: a case study of the California Sierra Nevada. *Journal of Hydrometeorology*, *18*(4),  
442 1101–1119.

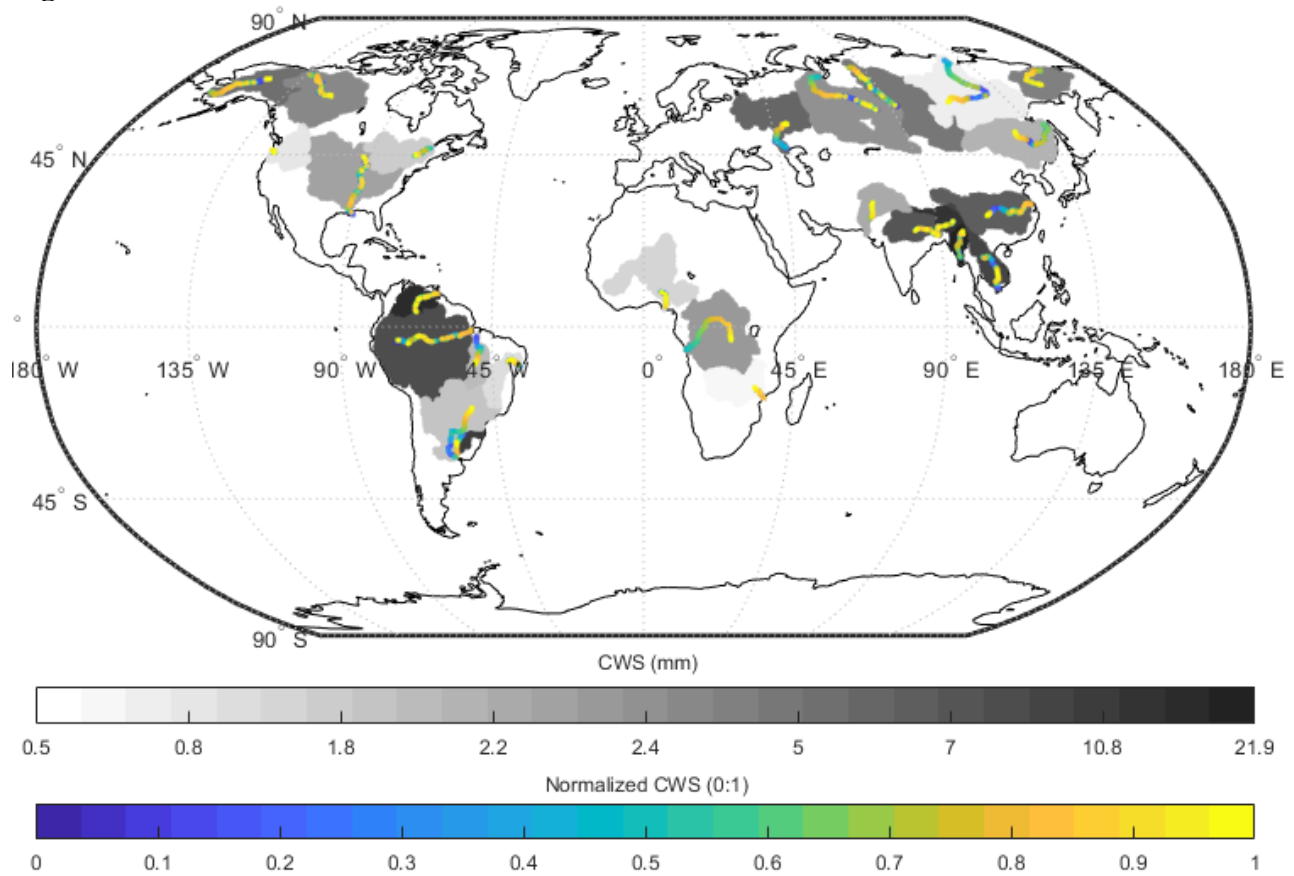
- 443 Yamazaki, D., Kanae, S., Kim, H., & Oki, T. (2011). A physically based description of  
444 floodplain inundation dynamics in a global river routing model. *Water Resources*  
445 *Research*, 47(4). <https://doi.org/10.1029/2010WR009726>
- 446 Yamazaki, D., Sato, T., Kanae, S., Hirabayashi, Y., & Bates, P. D. (2014). Regional flood  
447 dynamics in a bifurcating mega delta simulated in a global river model. *Geophysical*  
448 *Research Letters*, 41(9), 3127–3135. <https://doi.org/10.1002/2014GL059744>
- 449 Yamazaki, D., Trigg, M. A., & Ikeshima, D. (2015). Development of a global ~ 90 m water body  
450 map using multi-temporal Landsat images. *Remote Sensing of Environment*, 171, 337–  
451 351. <https://doi.org/10.1016/j.rse.2015.10.014>
- 452 Yang, X., T. M. Pavelsky, G. H. Allen, & G. Donchyts. (2019). RivWidthCloud: An Automated  
453 Google Earth Engine Algorithm for River Width Extraction From Remotely Sensed Imagery.  
454 *IEEE Geoscience and Remote Sensing Letters*, 1–5. <https://doi.org/10.1109/LGRS.2019.2920225>

455 **Figure 1.**

456

457 *Figure 1. Mississippi VCWS time series. Panel A is the complete record, while panel B shows*458 *constructed climatology (VCWSC). The Mississippi climatology amplitude (VCWSCA) is 7.1245*459 *km<sup>3</sup> while the drainage area is 3,244,506 km<sup>2</sup>. Dividing VCWSCA by drainage area results in a*460 *CWS of ~2.2mm.*

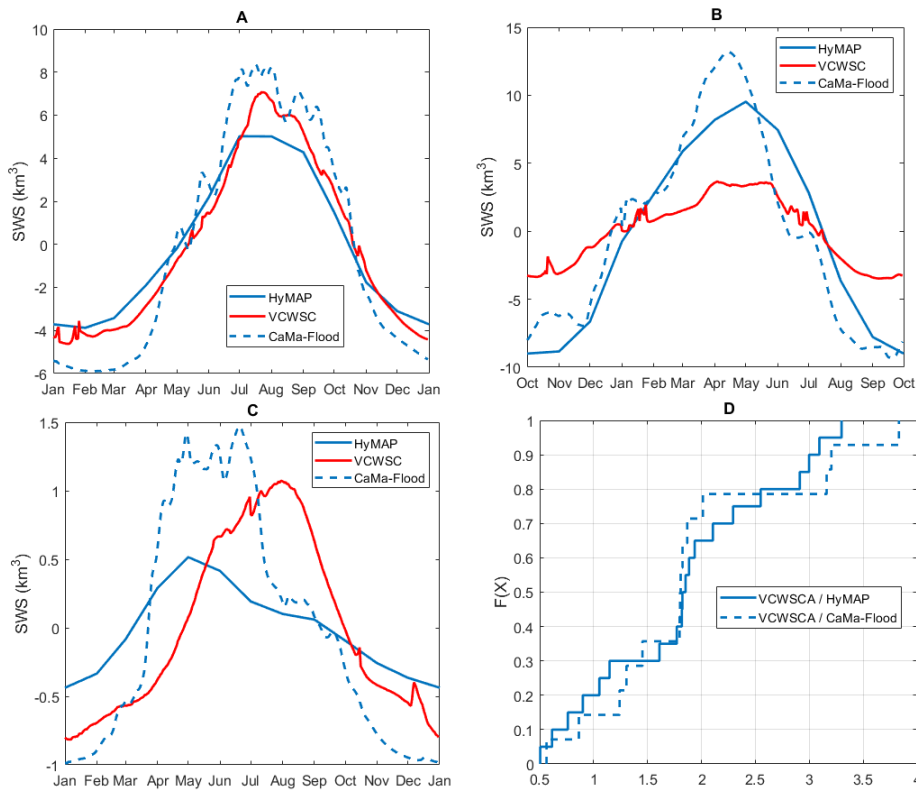
461 **Figure 2.**



462  
 463 *Figure 2. CWS (basin normalized VCWSCA in mm) shown in greyscale. Individual 1km VCWSCA*  
 464 *segment data shown in blue-yellow color scale rescaled between zero and 1 (following formula*  
 465 *S1) to highlight where rivers store their water. Every 100th point shown.*

466

467 **Figure 3.**



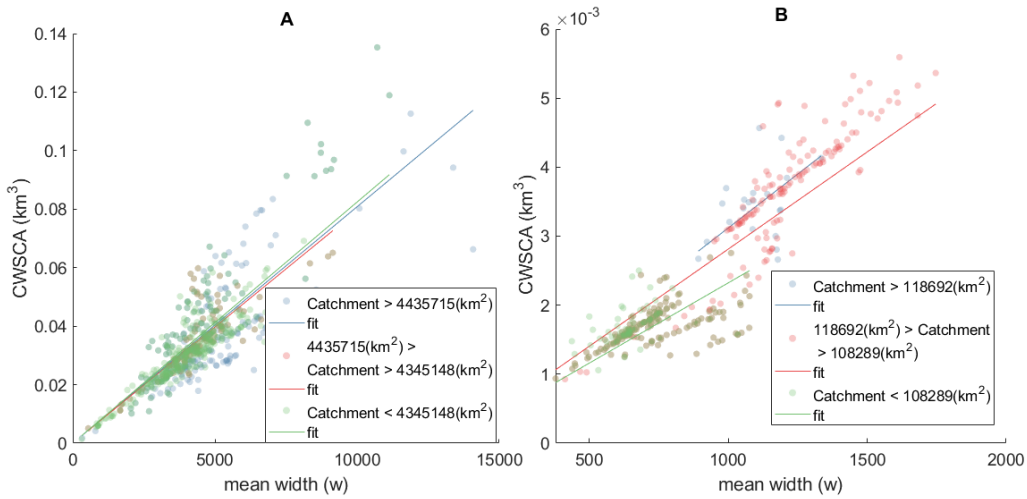
468

469 *Figure 3 Storage change climatology plots for the Brahmaputra (A), Mississippi (B), and Indus (C)*  
 470 *Rivers. HyMAP data is shown in solid blue, CaMa-flood is shown in dashed blue, and Measured*  
 471 *VCWSCA is shown in red panel D shows the CDF of amplitude ratio comparisons from both*  
 472 *models (amplitude ratios < 4).*

473

474 **Figure 4.**

475



476  
477

478 *Figure 4. VCWSCA and mean width plots for the Amazon (A) and Uruguay (B) basins. Data is*  
 479 *plotted by drainage area and fit with a least squares regression line per catchment regime. Data*  
 480 *is grouped by large increases in in flow accumulation to avoid comparison across large*  
 481 *tributaries. We then re-assimilated any divisions that did not achieve a change in basin drainage*  
 482 *area > 10 %.*

483

484

485 **Table 1.**

486 *Table 1 Percentage of GRACE TWS measure in main-stem CWS*

River	% GRACE TWS	Basin drainage area (km <sup>2</sup> )	CWS measured area (km <sup>2</sup> )	GRWL inundated area (km <sup>2</sup> )	CWS/ Width slope change with drainage area
Amazon	2.50	5,888,268	12,702	60,673	No
Amur	5.69	2,101,598	3,808	10,194	Yes
Ayeyarwada	5.29	385,438	1,449	3,199	No
Columbia	0.21	712,035	634	4,543	No
Congo	2.19	3,689,187	8,362	18,813	Yes
Ganges-Brahmaputra	3.02	1,792,035	5,293	15,160	No
Indus	2.20	864,062	935	4,330	-
Kolyma	2.43	657,254	1,928	5,150	-
Lena	0.51	2,467,695	9,507	20,836	-
Mackenzie	2.57	1,805,884	2,559	14,749	-
Mekong	2.89	773,231	2,244	18,197	Yes
Mississippi	1.69	3,244,506	2,709	17,002	Yes
Niger	0.45	2,115,246	642	7,019	-

Ob	1.71	2,929,051	4,757	15,176	-
Orinoco	4.96	937,352	2,899	7,537	No
Parana	1.12	2,639,954	6,096	20,843	Yes
SaoFrancisco	0.30	634,842	1,132	4,088	Yes
StLawrence	1.15	1,055,756	1,531	6,606	-
Tocantins	0.41	769,445	2,000	6,914	-
Uruguay	13.81	265,786	1,872	2,183	Yes
Volga	3.24	1,410,756	4,787	17,857	-
Yangtze	7.62	1,908,837	4,460	15,550	Yes
Yenisei	2.50	2,518,211	4,305	23,558	-
Yukon	1.42	1,373,188	2,067	6,687	-
Zambezi	0.05	1,373,188	504	7,186	Yes

487

488